COMPTES RENDUS

MECANIQUE

Combustion for aerospace propulsion

Injection coupling with high amplitude transverse modes: Experimentation and simulation

Yoann Mery [*], Sébastien Ducruix, Philippe Scouflaire, Sébastien Candel

École Centrale Paris, laboratoire EM2C, CNRS, 92295 Châtenay-Malabry, France

Abstract

High frequency combustion instabilities have technical importance in the design of liquid rocket engines. These phenomena involve a strong coupling between transverse acoustic modes and combustion. They are currently being investigated by combining experimentation and numerical simulations. On the experimental level, the coupling is examined in a model scale system featuring a multiple injector combustor (MIC) comprising five coaxial injectors fed with liquid oxygen and gaseous methane. This system is equipped with a novel VHAM actuator (Very High Amplitude Modulator) which comprises two nozzles and a rotating toothed wheel blocking the nozzles in an alternate fashion. This device was designed to obtain the highest possible levels of transverse oscillation in the MIC. After a brief review of the VHAM, this article reports cold flow experiments using this modulator. Velocity maps obtained under resonant conditions using the VHAM are examined at different instants during a cycle of oscillation. Experimental data are compared with numerical pressure and velocity fields obtained from an acoustic solver. The good agreement observed in the nozzle vicinity indicates that numerical simulations can be used to analyze the complex flow field generated by the VHAM. ***To cite this article: Y. Mery et al., C. R. Mecanique 337 (2009).***

© 2009 Académie des sciences. Published by Elsevier Masson SAS. All rights reserved.

Résumé

Couplage entre injection et modes transverses de grande amplitude : expérience et simulation. Les instabilités haute-fréquence ont une grande importance technique dans la conception des moteurs-fusées à ergols liquides. Ces phénomènes impliquent un couplage fort entre les modes acoustiques transverses et la combustion. Ils sont actuellement étudiés en combinant expériences et simulations numériques. Du point de vue expérimental, le couplage est examiné sur un système réduit comprenant une chambre à injecteurs multiples (MIC) munie de cinq injecteurs coaxiaux alimentés par de l'oxygène liquide et du méthane gazeux. Ce système est équipé d'un nouvel actionneur VHAM (Very High Amplitude Modulator) constitué de deux tuyères et d'une roue dentée qui bloque alternativement chacune des tuyères. Ce dispositif a été conçu pour obtenir les niveaux d'oscillation transverse les plus importants possibles dans le MIC. Après une rapide revue du VHAM, des expériences à froid utilisant ce modulateur sont présentées. Les champs de vitesse obtenus dans des conditions résonantes utilisant le VHAM sont examinés à plusieurs instants d'un cycle d'oscillation. Les données expérimentales sont comparées avec les champs de vitesse et de pression obtenus avec un code acoustique. Le bon accord observé dans le voisinage de la tuyère indique que la simulation numérique peut être utilisée pour analyser l'écoulement complexe généré par le VHAM. ***Pour citer cet article : Y. Mery et al., C. R. Mecanique 337 (2009).***

© 2009 Académie des sciences. Published by Elsevier Masson SAS. All rights reserved.

Keywords: Combustion; Acoustic coupling; High frequency instability; Injection

---

[*] Corresponding author.

E-mail address: yoann.mery@em2c.ecp.fr (Y. Mery).

1. Introduction

Combustion dynamics affecting many practical systems often involves very high acoustic levels. To understand, predict, and control such phenomena, one wishes to reproduce these high amplitudes with an external modulator. This raises difficult issues because the system has to operate under extreme conditions prevailing in combustors. In most cases, the use of loudspeakers is not possible because the driver unit will be in contact with high temperature gaseous streams at a very high mean pressure. These harsh conditions are typical of the model scale experiments carried out to study acoustic coupling with cryogenic jet flames [1]. One possible solution which is commonly adopted in propulsion applications consists in using fluidic actuator systems relying on rotating toothed wheels.

The present study concerns one such device which is specifically designed to examine interactions between transverse acoustic oscillations and cryogenic combustion. The modulator comprises a rotating toothed wheel periodically blocking the flow through a couple of nozzles. The modulator was initially installed on the lateral side of the MIC (Multiple Injector Combustor) and the wheel was used to block the flow through an auxiliary nozzle. Fig. 1(a) shows the principle of this initial set up. Propellants are injected through three or five coaxial injectors (liquid oxygen–gaseous/transcritical methane), and are ejected by the main exhaust nozzle. A secondary nozzle, located at the top of the chamber, is periodically blocked or set open by the toothed wheel inducing pressure oscillations in the chamber. This device was used to establish interactions between the flames and the transverse motion as described for example in [1]. Unfortunately, the level of oscillation of a few percent of the chamber pressure was too weak to trigger self-sustained instabilities. It also did not quite reproduce conditions which typically prevail in rocket engines when a transverse acoustic instability occurs.

It was assumed that higher levels of modulation could be obtained by modulating the total mass flow rate. The VHAM (Very High Amplitude Modulator) exploits this idea by making use of an arrangement in which the total mass flow rate injected in the chamber escapes through two nozzles blocked alternately by a toothed wheel (Fig. 1(b)). Propellants are still introduced in the chamber through five coaxial injectors. The wheel is designed so that a nozzle is shut when the other nozzle is open. Gases are exhausted from the chamber through one nozzle at a time. Since the wheel is turning, the gas stream is ejected successively from the top and from the bottom of the chamber. This induces a pressure drop at the operating nozzle and an acoustic wave is created by this process. The excitation of upper and lower regions of the chamber will favor transverse modes, providing strong resonances at the 1T and 1T1L eigenfrequencies which are typical of the transverse motion under combustion instability. Because the system operates on the total flow rate, it may be possible to generate much higher levels of modulation eventually reaching 20% of the mean pressure, levels which are typically observed in self-sustained liquid rocket instabilities.
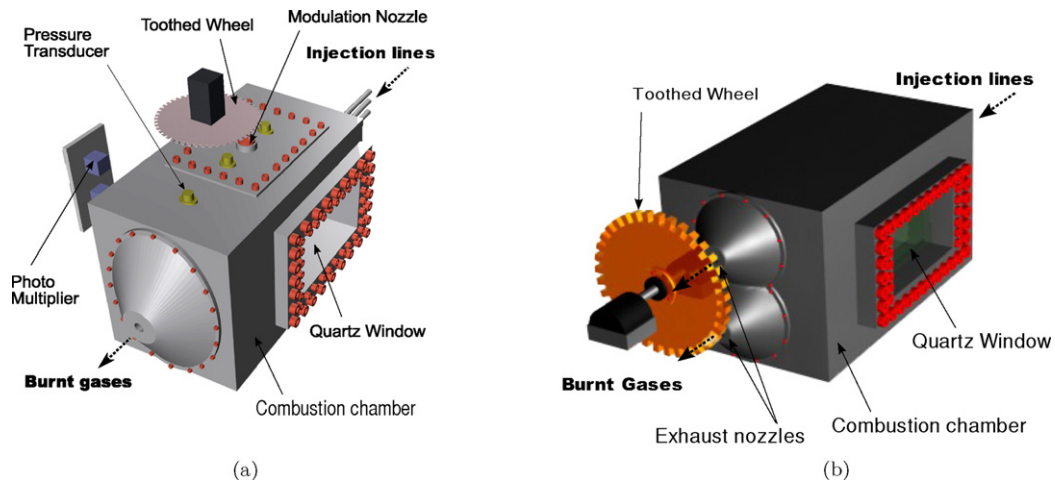

Fig. 1. (a) MIC equipped with a lateral toothed wheel modulator and diagnostics; (b) VHAM geometry.
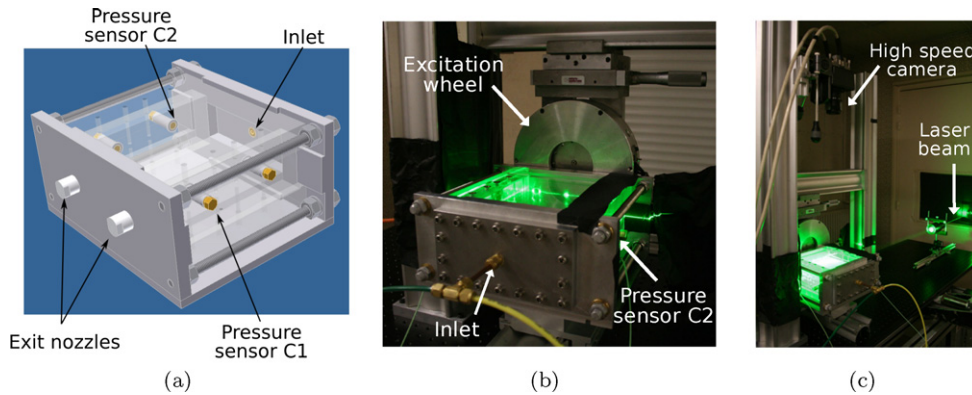
Fig. 2. General view of the experimental test bench: (a) Details of the transparent pressurized cavity; (b) View of the TPC equipped with the VHAM modulator; (c) Optical arrangement for PIV measurements.

The detailed design and manufacturing of the VHAM has been carried out at ONERA and the system has become operational in the fall of 2008. To assist this process, it was decided to develop experiments on a cold flow chamber pressurized with air at a moderate value of 2.5–3 bar, and equipped with a VHAM. The objective has been to examine the effect of operating parameters and to optimize their value in order to maximize the acoustic response in the chamber. Some geometrical parameters defining the VHAM (wheel diameter, thickness, materials, etc.) were selected on the basis of theoretical and numerical studies presented previously. Other parameters have been defined experimentally with another laboratory system which focused on the understanding of the influence of nozzle length and exit diameter as well as on the influence of mean pressure. This provided useful indications that helped define the full scale VHAM. Some comparisons between experiments and numerical simulation were also carried out previously [1].

The objective of the present cold flow system designated as the TPC (Transparent Pressurized Cavity) is to allow an experimental analysis of the unsteady velocity and pressure fields induced by the VHAM. The chamber is transparent with Plexiglas lateral walls providing complete optical access (see Fig. 2). This configuration can be used to perform time resolved PIV[1] measurements inside the cavity, using a procedure described in [2].

The TPC can be used to examine various questions. One first wishes to get a better understanding of the transfer of convective energy into acoustic energy and to examine effects of some geometrical parameters (such as nozzle exit diameters). Second, it is interesting to confirm that the velocity field is that corresponding to acoustic eigenmodes identified by the wall mounted pressure sensors. Third, it is also instructive to see if the flow field compares well with numerical simulations. Experiments on the TPC constitute an excellent test bench for validation of numerical acoustic codes. Another aspect which can be investigated is the sensitivity of confined jets to external modulations. It is known that free jets are quite susceptible to external acoustic perturbations [3], but much less is known about confined jets submitted to transverse excitation. The jet Strouhal number corresponding to the most amplified perturbations is typically controlled by a Strouhal number scaling rule: $St \simeq 0.3$. It is then interesting to examine the coupling between the jet and the transverse motion when the most amplified frequency coincides with that of the acoustic motion.

2. Experimental methods

Experiments are carried out in the setup shown in Fig. 2. The chamber is equipped with a single air injector and is operating at a nominal pressure $p_c = 2.5$ bar. The unsteady pressure is recorded by pressure sensors C1 and C2 located on the two sides of the TPC. The unsteady flowfield is deduced from high speed PIV measurements described in the next subsection. The modal identification method is examined subsequently.
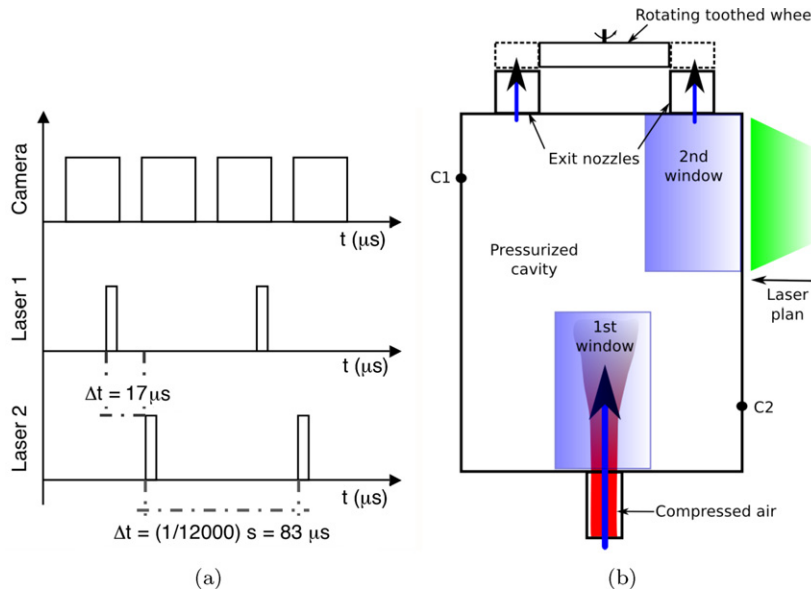
---

[1] Particle Image Velocimetry.

Fig. 3. (a) Time diagram for the time resolved PIV. (b) Zones of interest in the cavity.

2.1. Particle Image Velocimetry

Particle Image Velocimetry (PIV) [4,5] is used in the present investigation to determine the acoustic velocity field induced by the VHAM. The PIV arrangement is shown in Fig. 2(c). A horizontal laser sheet is transmitted into the TPC from the side. The flow is seeded with small oil droplets and illuminated by this light sheet. A CCD camera collects light scattered by the droplets. Two images of the flow are recorded at two instants in time separated by a short delay Δt. In processing the successive droplet images it is assumed that the droplet displacement is proportional to the local flow velocity. The droplet velocity can then be determined by measuring its displacement vector, $\Delta \boldsymbol{x}$, between two instants t and $t + \Delta t$, where Δt is the time delay between the two images of the seeded flow. The local droplet velocity will coincide with the local flow velocity if the droplet size is sufficiently small and the droplets follow the flow and its fluctuations with a negligible time lag. The local velocity of a droplet and consequently the local velocity of the flow is then given by $\boldsymbol{v}(\boldsymbol{x}, t) = \Delta \boldsymbol{x} / \Delta t$.

The chamber lateral walls are transparent so that the laser sheet can cross the cavity horizontally. The light sheet is generated by a system consisting of two Nd:YAG lasers (*Quantronix*), a laser beam recombining device and a set of cylindrical lenses (*Melles Griot*). Both lasers emit a pulse at a wavelength of 532 nm. The pulse energy and temporal width are 6 mJ and 160 ns respectively. Optics are used to combine both beams along the same trajectory. A set of lenses is used to transform the laser beam into a planar light sheet 90 mm wide and 0.3 mm thick. The camera Photron Fastcam APX can record 1024×1024 pixel images at a rate of 2000 frames per second. It is equipped with a 105 mm F/1.8 Nikon Nikkor objective and placed perpendicularly to the TPC axis.

The two lasers operating at 12 kHz and the camera operating at 24 kHz are synchronized by a pulse delay generator (*BNC* 555 pulse/delay Generator), as shown in the time trace diagram displayed in Fig. 3(a). In addition, tomographic experiments have been performed with a single laser pulsing at 12.5 kHz and the camera operating at the same rate.

At the rate of 24 kHz (for the camera), the size of the pictures must be reduced to 128×512 pixels, a limited size which will be improved using new generation systems. At a lower frequency of 12.5 kHz images have twice as many pixels (256×512). The airflow is seeded with oil droplets with a nominal diameter $d = 1$ μm. Using Ref. [4], one can estimate that the error introduced by the droplet time delay due to drag forces is less than 2%. By estimation of the maximum velocity, the time delay between the two pulses is chosen equal to $\Delta t = 17$ μs at the rate of 24 kHz for the camera.

At 12.5 kHz, with only one laser operating, PIV processing can still be used, but the time lapse (which is then $1/12.5 \times 10^3 \simeq 83$ μs) is too large to be able to cope with the highest velocities in the chamber. This mode of operation yields the same number of velocity fields as the 24 kHz tests but provides a double-sized window.

Table 1

PIV sampling and processing parameters. There are two image sizes and the region observed in the TPC can be modified.

Acquisition	Field-of-view	Image size	Camera pitch	Frequency	Nb images
	$x = 48$ mm or 24 mm; $y = 95$ mm	$[128 \times 512]$ pixels or $[256 \times 512]$ pixels	0.017 mm/px	12 kHz	24,000 or 12,000
Processing	Sub-pixel scheme	Initial window size	Final window size	Overlap	Nb of vectors
	Gaussian	$[32 \times 32]$ pixels	$[8 \times 8]$ pixels	25%	$[21 \times 85]$ or $[42 \times 85]$

The raw image pairs are exported and an off-line image processing is performed with an adaptive cross-correlation code ("Flow-Manager" from *Dantec*) using Fast Fourier Transform algorithms. The raw image pairs are divided into square interrogation windows having final dimensions of 8×8 pixels with an overlap of 25%. PIV analysis is optimized to deal with high velocity and density gradients, providing a peak finding error of less than 0.1 pixel in classical applications [6]. Parameters used for the time resolved PIV treatments are gathered in Table 1.

To get a suitable resolution, the camera has to be focused on specific regions of interest. Two domains identified as most representative of the flow dynamics are shown in Fig. 3(b):

(1) The chamber head region is used to observe the injected air stream and the acoustic field around the axial pressure node;
(2) The flow field in the nozzle vicinity provides indications on the region where the acoustic field is generated. It is interesting to examine this region and see if and how a gas element changes its trajectory when a tooth blocks the nozzle.

The influence of several parameters has been studied (nozzle exit diameters, mean pressure and backplane shape), and for each of these parameters, five tests have been carried out: (1) Flow without acoustic modulation; (2) Linear frequency sweep to find the eigenfrequencies; (3) Continuous wave operation at the 1L eigenfrequency; (4) Continuous wave operation at the 1T eigenfrequency; (5) Continuous wave operation at the 1T1L eigenfrequency. In each of these tests, three camera frequencies and two domains were explored. From the systematic tests carried out with this setup (3 parameters $\times$ 5 types of modulation $\times$ 2 camera frame rates $\times$ 2 domains = 60), we only discuss the most relevant results. The data confirms that the mass flow rate, controlled by the nozzle diameters, is the parameter with the most critical influence on the level of modulation. Results discussed in the next section were obtained with the largest nozzle diameter.

2.2. Acoustic mode identification

The modal eigenfrequencies are determined by imposing a constant acceleration to the wheel. The frequency is swept linearly from 0 to 2600 Hz. Signals recorded by the pressure transducers are then processed to determine the short time spectral density and identify the eigenmodes. Continuous Wave (CW) modulation tests are then carried out to excite the 1T and 1T1L eigenmodes.

Fig. 4(a) shows results of a linear frequency modulation. Four resonance peaks emerge above the background noise. The two highest peaks respectively correspond to the 1T mode ($t \simeq 7000$ ms) and to the 1T1L mode ($t \simeq 8500$ ms). To identify the eigenmodes, one can use a short time Fourier analysis as exemplified in Fig. 4(b). This figure displays the spectral content of the signal as a function of time. The horizontal and vertical axis correspond to time and frequency respectively while the color contours represent the amplitude of the short time Fourier transform of the signal recorded by a pressure transducer. Hence, the main straight line in the graph is the linear modulation, and the red areas correspond to frequencies where the chamber resonates.

High speed PIV provides a large number of instantaneous velocity fields. The data presented in this article are obtained by digital processing of more than 6000 instantaneous velocity fields for each case. To observe the 1T mode, for example, the wheel is turned on and brought to a fixed angular velocity corresponding to the frequency of the 1T mode of the cavity (here, $f_{1T} = 1215$ Hz). The high speed camera coupled with the laser records a specified number M of periods.
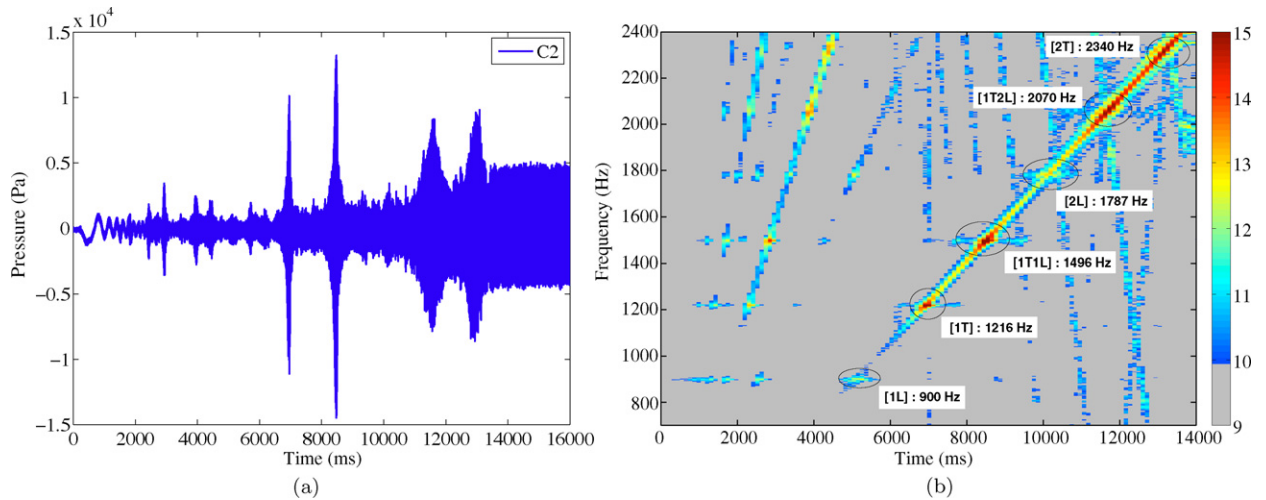
Fig. 4. (a) Time trace of the signal recorded by a side mounted pressure transducer. The frequency is swept linearly from 0 to 2600 Hz. (b) Short time power spectral density. The frequency is swept linearly from 0 to 2600 Hz.

For a frame rate of 24,000 images per second one obtains 12,000 velocity fields per second. For the 1T mode one gets $12,000/1215 \simeq 10$ fields per period. Since each instantaneous field also includes effects of turbulent fluctuations and some noise, it is interesting to use conditional sampling and add up images corresponding to the same phase in the cycle. This extracts the acoustic velocity field from the background noise and eliminates the turbulent fluctuations. The phase conditioned results are smooth and easier to interpret as exemplified in Figs. 6(a) and (b). Formally, the velocity field can be cast in the form:

$$\boldsymbol{v}(t) = \boldsymbol{v}_a + \boldsymbol{v}_t + \boldsymbol{v}_c + \boldsymbol{n}$$
$$\bar{\boldsymbol{v}} = \overline{\boldsymbol{v}_a} + \overline{\boldsymbol{v}_c} + \bar{\boldsymbol{n}}$$

where $\boldsymbol{v}_a$, $\boldsymbol{v}_t$ and $\boldsymbol{v}_c$ respectively correspond to acoustic, turbulent, mean flow velocities while $\boldsymbol{n}$ represents measurement noise. One expects that phase-averaging will reduce the noise component while the turbulent fluctuations will be averaged out. Thus $\bar{\boldsymbol{v}}$ will essentially contain the mean flow velocity which is quite small in most of the domain and the average of the acoustic velocity over a small phase interval $[\phi_1 \; \phi_2]$ around the phase used to record each instantaneous image:

$$\bar{\boldsymbol{v}}(\phi) \simeq \frac{1}{N} \sum_{\phi \in [\phi_1 \; \phi_2]} \boldsymbol{v}(\phi)$$

where N is the total number of fields having a phase in the range $[\phi_1 \; \phi_2]$. One expects to find $\bar{\boldsymbol{n}} = 0$ but the bias introduced by the measurement technique is not arbitrary and the corresponding error can grow when N becomes very large. If the experiment is done correctly, this phenomenon only occurs in limited regions which can be easily identified and eliminated manually.

3. Flow configuration in the jet vicinity

3.1. Velocity fields

The jet neighborhood is examined in this section by aiming the camera at the first window (see Fig. 5(a)). The velocity field represented in Fig. 5(b) defines the nominal operating conditions. The mean pressure is $p \simeq 2.5$ bar, the diameter of the exhaust nozzles is $\phi = 1.8$ mm. First, the jet without modulation is studied. One of the exhaust nozzles is closed so that the mass flow rate has the same order of magnitude as that obtained when the wheel is rotating (the wheel shuts one nozzle after the other). The jet spreading angle is relatively small and the maximum velocity on the jet axis is about 16 m s^{-1}. Note that axis x^* and y^* represents mm in the reference of each window.
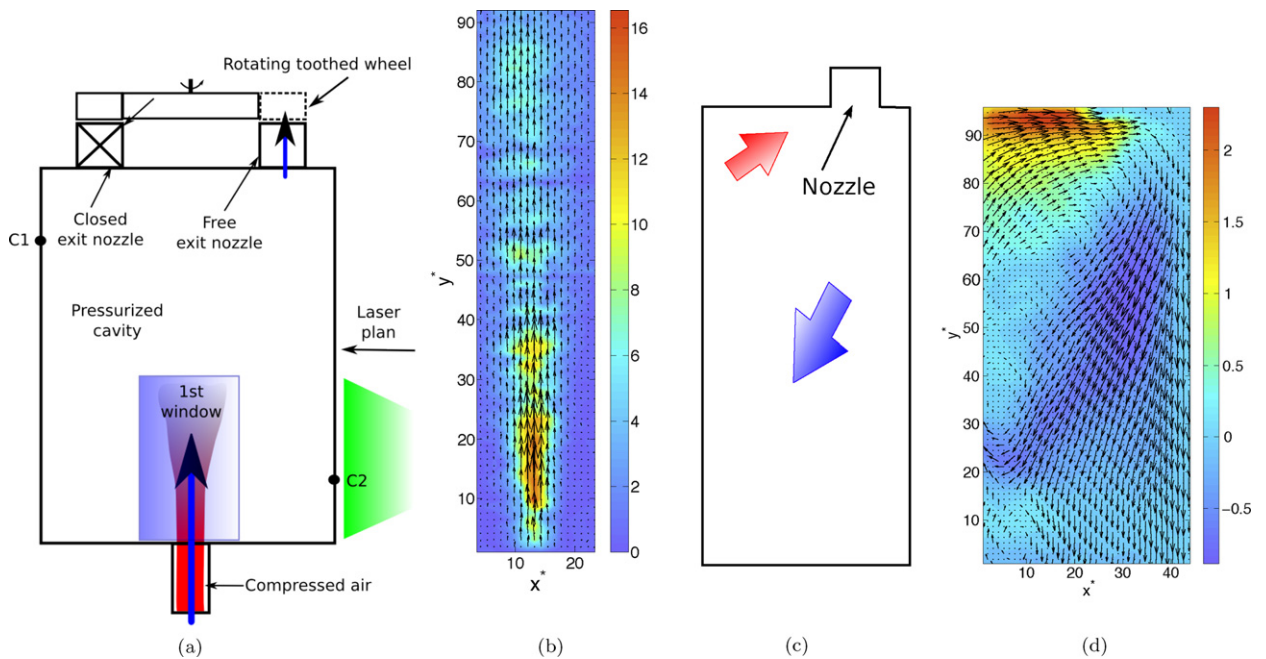
Fig. 5. (a) Experimental configuration for a steady flow test; (b) Contour plot of the axial flow velocity in the jet (m s^{-1}); (c) Schematic representation of the PIV window near the nozzle; (d) Mean flow field without excitation colored by transverse velocity near the nozzle (m s^{-1}).

Figs. 6(a) and (b) display velocity distributions during a period for the 1T and 1T1L modes respectively. Arrows show the direction of the flow, the background color represents the local transverse velocity. This component oscillates between -3 and 6 m s^{-1} for the 1T mode and between -3.5 and 5 m s^{-1} for the 1T1L mode (the bias of the velocity vectors towards the right direction is due to a slight dissymmetry of the wheel mounting with respect to the nozzles). These values are relatively important compared to the mean injection velocity of 16 m s^{-1}. The plots indicate that the flow oscillates from left to right in both cases, which confirms that the motion corresponds to transverse modes. The most important difference between the two unsteady flow fields is that, for the 1T mode, the transverse velocity is always rather constant in the whole domain whereas for the 1T1L mode the velocity amplitude is close to zero at the top of the domain. These differences can be understood by examining numerical simulations, which will be described in Section 5.

It is also interesting to consider the shape of the jet injected into the TPC. Compared with Fig. 5(b), the angle is larger and the jet spreads more rapidly. This finding is discussed in Section 3.2.

3.2. Hydrodynamic instabilities

It is natural to examine the possible coupling between the jet hydrodynamic instabilities and the external acoustic modulation. It is known that the initial velocity difference between the jet and the surrounding environment creates a shear region in which the inflectional velocity profile gives rise to instabilities. This phenomenon may intervene in the mechanism of combustion instability. There are fundamental experiments on this topic [7] and this issue is reviewed in [8] and [9]. It is then logical to see if a resonant coupling is possible between transverse acoustic modes and hydrodynamic instabilities.

The growth rate of hydrodynamic instabilities is controlled by a Strouhal number $St = f D/U$, where f is the frequency, D is the jet diameter, U is the jet velocity and St is the Strouhal number. Experiments on air jets at moderate Reynolds numbers between 100 and 10^4 [7], indicate that the growth rate of hydrodynamic instabilities reaches its highest value for a Strouhal number of 0.3. This defines the preferred mode of instability of a free jet. For a diameter $D = 4$ mm, an injection velocity $U \simeq 16$ m s^{-1} and taking $St = 0.3$ one obtains a preferred frequency of $f = 1200$ Hz which nearly coincides with the 1T eigenfrequency. The spreading angle at the injector exhaust has been measured and is much larger than that corresponding to a naturally developing jet. The jet instability mode is clearly
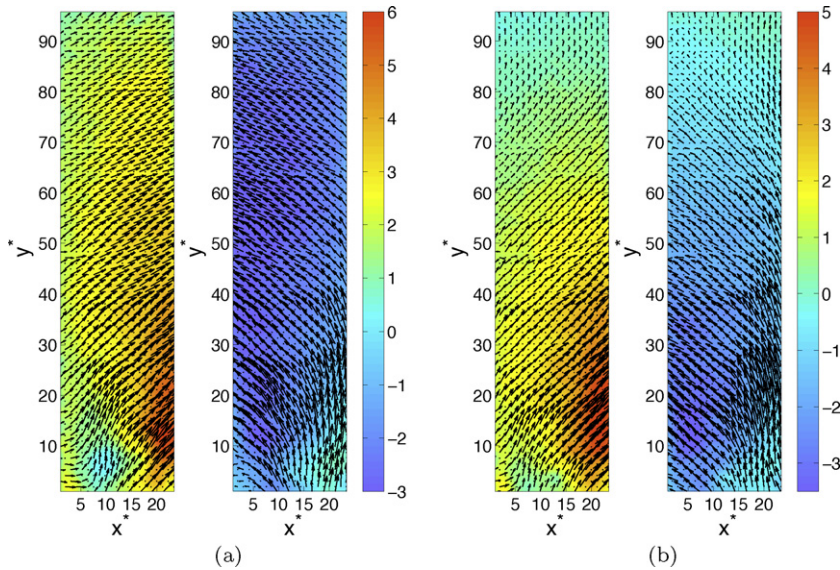
Fig. 6. Velocity field in the jet vicinity at two phases in a cycle. The transverse velocity is shown on a color scale $(\mathrm{m\,s^{-1}})$: (a) Modulation at 1215 Hz (1T mode); (b) Modulation at 1453 Hz (1T1L mode).

excited. When the excitation frequency is shifted from the eigenfrequency of the cavity, the amplitude of modulation is weaker and the jet spreads as if it were not submitted to an external forcing. The amplitude of modulation has the greatest influence on the spreading angle.

The 1T1L mode ($f = 1453$ Hz) features a very high amplitude of modulation. At this frequency the spreading angle is as important as that corresponding to the 1T mode, indicating that the jet is also receptive over a range of Strouhal numbers surrounding $St = 0.3$. The receptivity of the system is broad and the jet spreading angle remains high even when the modulation frequency differs from the preferred jet frequency.

This short analysis gives some useful information on the coupling between hydrodynamics and acoustics. The interaction modifies the jet shape even when the acoustic frequency does not exactly coincide with the preferred hydrodynamic frequency, as long as the wave amplitude is important enough.

4. Flow configuration in the nozzle vicinity

The nozzle area plays a key role in the VHAM operation. The toothed wheel closes the nozzle exit periodically, creating a source in the nozzle convergent which generates an acoustic field in the chamber. This process is now characterized by determining the velocity distribution near the nozzle entrance.

4.1. Velocity fields

Velocity distributions were recorded at a frame rate of 12.5 kHz because the maximum velocity is lower and can be accurately resolved by using successive images in the sequence. The window size is in this case twice that used previously.

The mean flow field is shown in Fig. 5(d). Since the cavity pressure is around 3 bar and the ambient pressure is 1 bar near the nozzle exit, the flow is naturally oriented outwards (and the nozzle throat is sonic). The mean field indicates that the nozzle acts like a sink and that most of the flow is recirculating. An instantaneous velocity field shows that there are many vortices in the cavity.

Figs. 7(a) and (b) show the velocity field at two instants of a cycle for the two modulation frequencies. The field is organized by the acoustic perturbation, and the vortices have been averaged out.

These figures indicate that close to the nozzle, the velocity changes its direction and the flow field is directed inwards during one half period and outwards during the next half period. The velocity levels reached in this oscillation
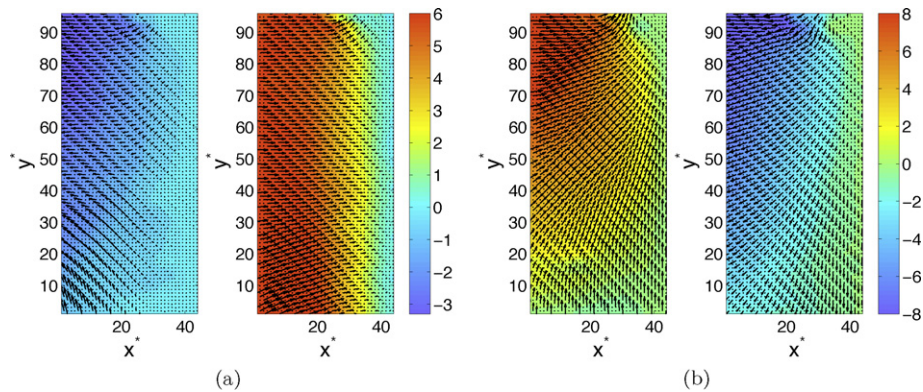
Fig. 7. Velocity field in the vicinity of the nozzle at two phases in a cycle. The transverse velocity is shown on a color scale (m s^{-1}): (a) Modulation at 1225 Hz (1T mode). In the first field the velocity vectors point away from the nozzle; (b) Modulation at 1461 Hz (1T1L mode). In the second field the velocity vectors point away from the nozzle.

are quite significant with a maximum of 8 m s^{-1} for the 1T1L mode. This inversion of velocity direction corresponds to the presence of a tooth which creates a local pressure increase propagating inwards and an oscillatory velocity field.

Spatial features of the velocity fields for the two modes are similar to what was already observed in the injection region. For the 1T mode, the acoustic velocity is essentially transverse. The velocity node is located at the lateral sides of the rectangular cavity. For the 1T1L mode, velocity vectors originate from the left and bottom of the window, which suggest that the node of the velocity field is the corner of the cavity. This explains why this mode is particularly well excited since the excitation point is close to the velocity node and the pressure antinode.

4.2. Pressure and velocity consistency

The pressure signals displayed in Fig. 8 are measured at the wall of the cavity by two sensors C1 and C2 at locations shown in Fig. 2(a). The transverse velocity signal is measured at a point located at $x^* = 13$ mm and $y^* = 77.8$ mm in the window defined in the nozzle vicinity. This velocity component is multiplied by $\rho_0 c$ to allow direct comparisons with the pressure waveform. For the 1T excitation, the signals detected by C1 and C2 are out phase. As expected the velocity signal is in quadrature with the pressure signal detected by sensor C2. It is interesting to note that the various signals have the same level indicating that $\rho_0 c$ suitably represents the scaling between pressure and velocity. This also indicates that pressure measured by wall transducers and velocity determined by PIV are consistent.

5. Comparison with numerical results

It is now worth seeing if the experimental data gathered in the TPC can be retrieved from numerical calculations based on an acoustic solver. AVSP is used to this purpose in the VHAM geometry with the aim of calculating the pressure and velocity fields associated with the TPC eigenmodes. AVSP is an acoustic code developed by CERFACS that solves Helmholtz equation. More information on this software can be found in a recent article [10].

The mesh used for the present calculations comprises $\simeq 90{,}000$ cells. Rigid wall conditions are used as boundary conditions. The nozzle walls also define velocity nodes but the exhausts are treated by imposing a reduced acoustic admittance: $\beta_* = (\gamma - 1)/2$, where $\beta = (u'/\bar{u})/(p'/\bar{p})$ [11]. This expression describes the response of a compact choked nozzle to longitudinal pressure waves. The temperature is fixed at 300 K, the mean pressure equals 2.5 bar, and $\gamma = 1.4$.

The fields are determined with AVSP for the different eigenmodes. Fig. 9 shows the spatial structure of the transverse velocity for the 1T and 1T1L modes. An important feature of these modes is the antinode locations. For the 1T mode, velocity is maximum on the chamber symmetry axis and the transverse velocity is nearly the same in each constant y section. The 1T1L mode does not have this property. The transverse velocity is strongest near the cavity head and backplane and vanishes near the cavity center.

A comparison with experimental results displayed in Figs. 6(a) (mode 1T) and (b) (mode 1T1L) indicates that these spatial characteristics are well retrieved. For the 1T mode (Fig. 6(a)), the transverse velocity represented by the
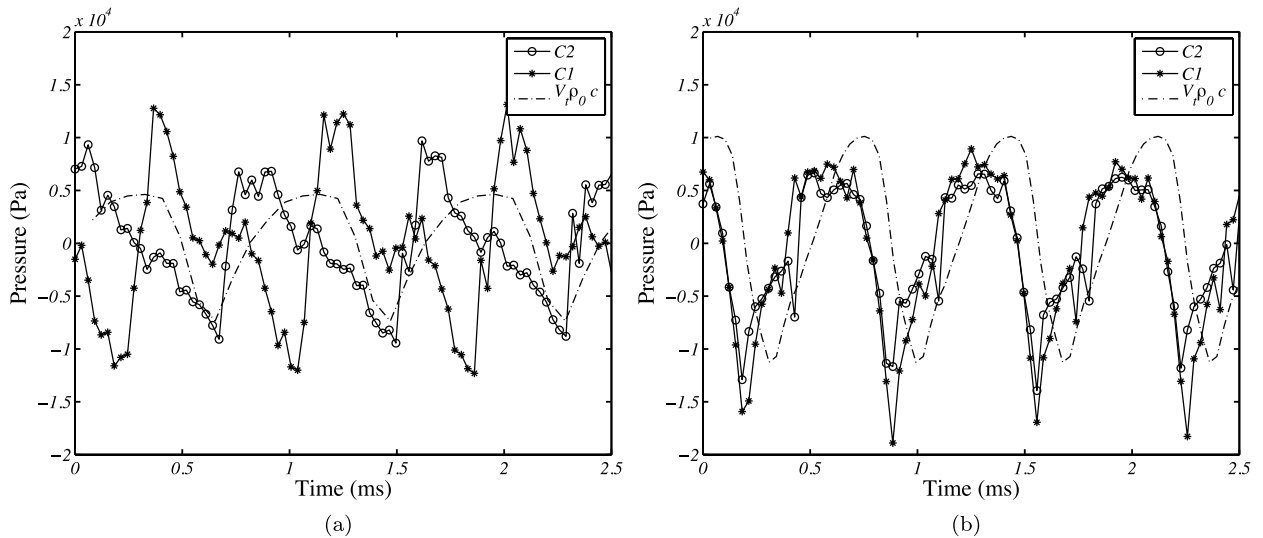
Fig. 8. Pressure evolution recorded by the C1 and C2 transducers plotted with the velocity evolution at point $x^* = 13$ mm and $y^* = 75.8$ mm of the field: (a) 1T mode, $f = 1225$ Hz; (b) 1T1L mode, $f = 1461$ Hz.
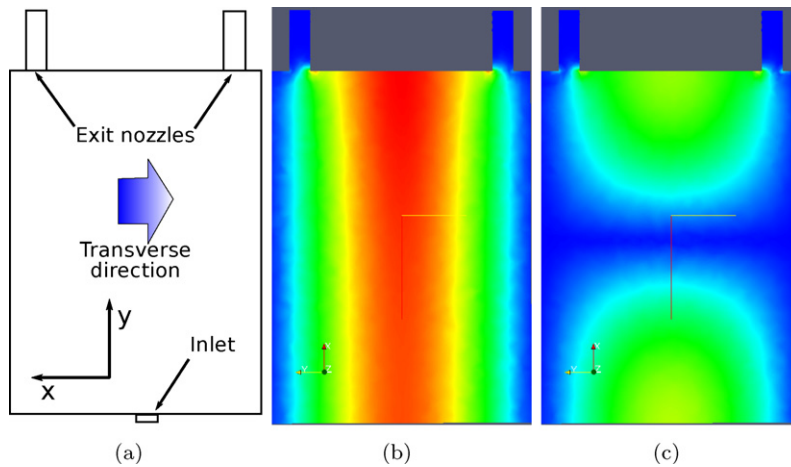

Fig. 9. Transverse velocity field for the 1T mode (b) and the 1T1L mode (c) computed with AVSP (arbitrary units).

color levels is almost uniform over the whole window. In contrast, in Fig. 6(b), the horizontal velocity is not only non-uniform, but it also has the features observed in the computations: the highest velocity is near the injection plane and the velocity near the center of the cavity (corresponding the top of the window), is constant and nearly vanishes.

Considering the second observation window located near the nozzle, the comparison between computation and experiment gives complementary elements and a good agreement is also observed. In addition, Fig. 7(a) (phase 2) shows that the transverse velocity is clearly uniform and does not depend on y, in distinction with what is observed in Fig. 7(b) for which, once again, the velocity field distribution depends on the two spatial coordinates.

Finally, in the close vicinity of the exit nozzle, comparison with computational results is not straightforward (Fig. 10). Physical phenomena in the nozzle region are difficult to describe only in acoustics terms. The compact nozzle impedance boundary condition used in the calculations does not reflect the complex processes induced by the rotating wheel. An exchange of energy takes place inside the nozzle giving rise to the pressure and velocity fields in the chamber. One should not expect a perfect match between simulation and experiments. However, the calculated velocity patterns in Figs. 10(a) and (c) are very close to the measured ones displayed in Figs. 10(b) and (d) for the 1T and 1T1L modes respectively.
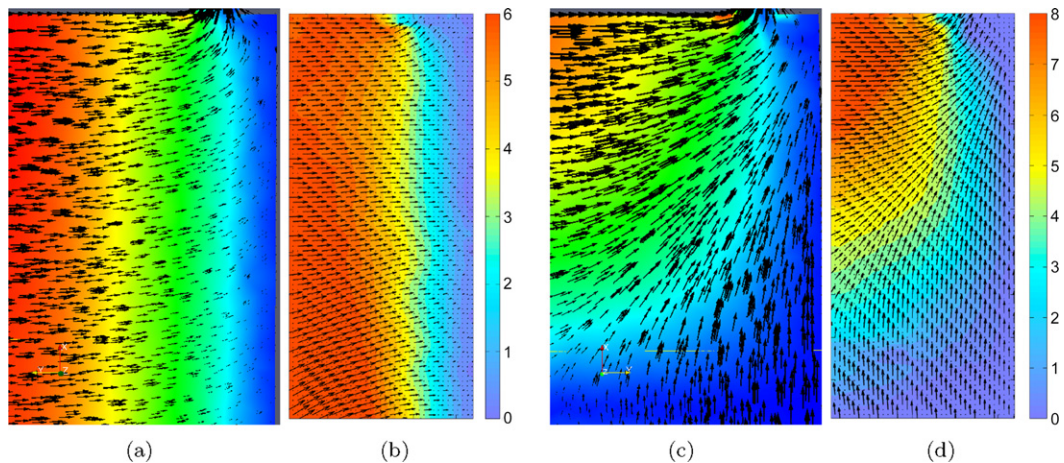
Fig. 10. Comparisons between experimental and numerical results for the window located in the vicinity of the exhaust nozzle. The transverse velocity field is displayed on a color scale. Arrows show the velocity vectors: (a) Calculated field corresponding to the 1T mode; (b) Measured field corresponding to the 1T mode $(m\,s^{-1})$; (c) Calculated field corresponding to the 1T1L mode; (d) Measured field corresponding to the 1T1L mode $(m\,s^{-1})$.

6. Conclusion

This article has focused on the structure of pressure and velocity fields generated by the Very High Amplitude Modulator (VHAM). This actuator was designed to generate large amplitude oscillations to allow detailed investigations of high-frequency coupling between transverse acoustic modes and cryogenic flames. The VHAM system is here mounted on a Transparent Pressurized Cavity (TPC) allowing measurements of the velocity field with high speed PIV and providing pressure records at the walls. It is shown that acoustic waves can reach high amplitudes when the system is brought to resonance at the 1T and 1T1L eigenfrequencies. The flow induced by the VHAM has the expected structure and features large velocity fluctuations. It is shown that modulation close to the most amplified jet hydrodynamic frequency augments the jet spreading angle. Velocity distributions are determined numerically with an acoustic solver together with a compact nozzle impedance condition. While transfer of energy taking place in the nozzles is quite complex, it is found that the calculated and experimental velocity patterns are in good agreement.

Acknowledgements

References

[1] F. Richecoeur, Expérimentations et simulations numériques des intéractions entre modes acoustiques transverses et flammes cryotechniques, Ph.D. thesis, Ecole Centrale Paris, December 2006.
[2] S. Barbosa, P. Scouflaire, S. Ducruix, Time resolved flowfield, flame structure and acoustic characterization of a staged multi-injection burner, Proceedings of the Combustion Institute 32 (2009) 2965–2972.
[3] A.L. Birbaud, D. Durox, S. Ducruix, S. Candel, Dynamics of free jets submitted to upstream acoustic modulations, Physics of Fluids 19 (1) (2007), Article 013602, 20 pp.
[4] R.J. Adrian, Particle-imaging techniques for experimental fluid-mechanics, Annual Review of Fluid Mechanics 23 (1991) 261–304.
[5] R.J. Adrian, Twenty years of particle image velocimetry, in: International Symposium on Applications of Laser Techniques to Fluid Mechanics, Lisbon, July 2004.
[6] J. Westerweel, D. Dabiri, M. Gharib, The effect of a discrete window offset on the accuracy of cross-correlation analysis of digital PIV recordings, Experiments in Fluids 23 (1) (1997) 20–28.
[7] S.C. Crow, F.H. Champagn, Orderly structure in jet turbulence, Journal of Fluid Mechanics 48 (1971) 547.
[8] C.M. Ho, P. Huerre, Perturbed free shear layers, Annual Review of Fluid Mechanics 16 (1984) 365–424.

[9] A. Ongoren, D. Rockwell, Flow structure from an oscillating cylinder. 2. Mode competition in the near wake, Journal of Fluid Mechanics 191 (1988) 225–245.

[10] F. Nicoud, L. Benoit, C. Sensiau, T. Poinsot, Acoustic modes in combustors with complex impedances and multidimensional active flames, AIAA Journal 45 (2) (2007) 426–441.

[11] F.E. Marble, S.M. Candel, Acoustic disturbance from gas non-uniformities convected through a nozzle, Journal of Sound and Vibration 55 (2) (1977) 225–243.